E&G Quaternary Sci. J., 75, 19–32, 2026
https://doi.org/10.5194/egqsj-75-19-2026


Open Access E&G Quaternary Science Journal

Research article

# Beryllium-10-derived denudation rates in the Roda Catchment, Germany

**Lianqing Zhang[1], Yingkui Li[2], Oscar Marchhart[3], Silke Merchel[3], Alexander Wieser[3], and Roland Zech[1]**

[1]Institute of Geography, Friedrich Schiller University Jena, 07743 Jena, Germany
[2]Department of Geography & Sustainability, University of Tennessee, Knoxville, TN 37996, USA
[3]Faculty of Physics – Isotope Physics, University of Vienna, 1090 Vienna, Austria

**Correspondence:** Lianqing Zhang (lianqingzhang2023@gmail.com)

**Relevant dates:** Received: 14 September 2025 – Revised: 28 December 2025 – Accepted: 27 January 2026 – Published: 12 February 2026

**How to cite:** Zhang, L., Li, Y., Marchhart, O., Merchel, S., Wieser, A., and Zech, R.: Beryllium-10-derived denudation rates in the Roda Catchment, Germany, E&G Quaternary Sci. J., 75, 19–32, https://doi.org/10.5194/egqsj-75-19-2026, 2026.

**Abstract:** Denudation is a key geomorphological process shaping landscapes. In-situ-produced cosmogenic $^{10}$Be has been used to quantify millennial denudation rates worldwide. Long-term denudation rates in the European lowlands can provide valuable insights into the roles of periglacial processes and human activity in landscape evolution. Here, we quantify local and catchment-wide denudation rates in the Roda Catchment in Thuringia, central Germany. Specifically, we constrain 17 catchment-wide denudation rates based on $^{10}$Be concentrations in river sediments and 5 local denudation rates based on $^{10}$Be concentrations from soil samples on the flat catchment divides. Catchment-wide denudation rates vary between $23.8 \pm 5.4$ and $79 \pm 18$ mm kyr$^{-1}$, and local denudation rates range from $23.4 \pm 5.6$ to $41.9 \pm 9.8$ mm kyr$^{-1}$. These catchment-wide denudation rates are consistent with published European data, which are generally higher than those reported from other regions worldwide. This difference can be attributed to periglacial dynamics during the last glacial period. The $^{10}$Be-derived long-term denudation rates in Europe are generally higher than recent, short-term erosion rates, despite vast human activities and intensive land use in recent decades. This could be due to past periglacial activity; large-scale forest clearance during the Roman and Medieval times; and the limitations of short-term measurements in capturing low-frequency, high-magnitude events. The observed differences between catchment-wide and local denudation rates suggest that denudation has led to changes in topographic relief in the Roda Catchment at a mean rate of 0–28 mm kyr$^{-1}$ over the past 10 ka.

**Kurzfassung:** Denudation ist ein zentraler geomorphologischer Prozess der Landschaftsformung. In-situ produziertes kosmogenes $^{10}$Be wurde mittlerweile nahezu weltweit gemessen, um Denudationsraten auf der Zeitskala von Jahrtausenden zu bestimmen. Entsprechende Daten aus den Mittelgebirgen und Tieflandregionen Europas könnten wertvolle Informationen über den Einfluss periglazialer Prozesse und menschlicher Aktivitäten auf die Landschaftsentwicklung liefern. In dieser Studie quantifizieren wir auf Einzugsgebietsebene gemittelte, sowie lokale Denudationsraten im Roda-Einzugsgebiet in Thüringen, Deutschland. Grundlage hierfür sind 17 $^{10}$Be-Konzentrationen in Flusssedimenten, bzw. in 5 Bodenproben von den flachen Wasserscheiden. Die Denudationsraten liegen zwischen $23{,}8 \pm 5{,}4$ und $79 \pm 18$ mm kyr$^{-1}$, bzw. $23{,}4 \pm 5{,}6$ und $41{,}9 \pm 9{,}8$ mm kyr$^{-1}$. Während die Werte gut mit pub-

lizierten Daten aus Europa übereinstimmen, sind sie höher als in anderen Regionen weltweit, was auf periglaziale Dynamik während der letzten Eiszeit zurückgeführt werden kann. Langfristige $^{10}$Be-Denudationsraten in Europa scheinen außerdem höher zu sein als rezente, kurzfristige Erosionsraten, trotz intensiver Landnutzung und menschlicher Eingriffe in den letzten Jahrzehnten. Mögliche Erklärungen sind periglaziale Prozesse, großflächige Waldrodungen in römischer und mittelalterlicher Zeit, sowie die begrenzte Aussagekraft kurzfristiger Messungen bei seltenen, ereignisreichen Prozessen. Die Unterschiede zwischen auf Einzugsgebietsebene gemittelten versus lokalen Denudationsraten deuten zudem darauf hin, dass die Denudation im Roda-Einzugsgebiet während der letzten 10 ka Reliefveränderungen mit durchschnittlich 0–28 mm kyr$^{-1}$ bewirkt hat.

## 1 Introduction

Denudation is associated with various physical, chemical, and biological processes that can shape landscapes (Allen, 2008). Quantifying denudation rates is important for investigating landscape evolution and its controls. Conventional approaches to estimating denudation rates at catchment scales are mainly based on field measurements of dissolved and suspended loads in streams, typically over timescales of decades (e.g., Clayton and Megahan, 1986). However, such gauging approaches may fail to capture rare extreme events, and the derived denudation rates may not represent denudation rates over geological (millennial) timescales (Milliman and Meade, 1983; Lenzi and Marchi, 2000; Granger and Riebe, 2014).

In-situ-produced cosmogenic nuclides can be used to constrain long-term denudation rates in a variety of settings (Nishiizumi et al., 1986; Lal, 1991; Bierman and Turner, 1995; Brown et al., 1995; Bierman and Steig, 1996; Granger et al., 1996). The principle of this method is that concentrations of cosmogenic nuclides are inversely proportional to the denudation rate of an eroding surface (Nishiizumi et al., 1986; Lal, 1991). Cosmogenic nuclides were initially used to quantify local bedrock denudation and soon extended to the catchment scale to estimate catchment-wide denudation rates from nuclide concentrations in river sediments (Brown et al., 1995; Bierman and Steig, 1996; Granger et al., 1996; von Blanckenburg, 2005). Since then, in-situ-produced cosmogenic nuclides, particularly $^{10}$Be measured in quartz, have been widely used to constrain denudation rates at the catchment scale.

Previous studies have shown that denudation rates are influenced by various factors, including topography, climate, vegetation, lithology, and tectonics. Carretier et al. (2013), for example, used both suspended-load measurements and $^{10}$Be-derived denudation rates along an exceptional climatic gradient in the Andes of central Chile and found that slope is the primary control on denudation. Based on data for the European Alps, Delunel et al. (2020) also highlighted a close relationship between slope and denudation. The effects of precipitation and vegetation on denudation remain controversial. Starke et al. (2020) found both positive and negative correlations between denudation and vegetation using 86 $^{10}$Be-derived denudation rates along the western Andean margin. These contrasting observations have been interpreted as resulting from competing effects of precipitation and vegetation on denudation. The complex interactions between climate, vegetation, and denudation have also been proposed by Mishra et al. (2019) and Chen et al. (2022) using global data. Tectonic forcing can significantly accelerate physical erosion and chemical weathering (Riebe et al., 2001; von Blanckenburg, 2005). Temperature-controlled glacial and periglacial erosion processes play an important role in limiting orogen elevations and thereby shaping landscapes (Roda-Boluda et al., 2023). Frost cracking has been identified as a key driver of denudation in the European Alps and other mid-elevation mountain ranges (Delunel et al., 2010). Lithology, as an indicator of bedrock strength, can also exert an important control on denudation (Palumbo et al., 2010; Portenga and Bierman, 2011; Scharf et al., 2013; Ott, 2020).

Cosmogenic-nuclide-derived denudation rates have also been used to explore topographic relief changes. For example, Li et al. (2014) found that the landscape has been relatively stable on the central Tibetan Plateau, while its margins are affected by active fluvial erosion based on $^{10}$Be-derived denudation rates across the Tibetan Plateau and its bordering mountains. The difference between catchment-wide and local denudation rates from flat catchment divides can be used to evaluate topographic relief changes due to denudation over geological timescales (e.g., Hancock and Kirwan, 2007; Meyer et al., 2010b; Wolff et al., 2018; Heineke et al., 2019; Hetzel et al., 2024). Although denudation rates and associated topographic changes have been widely investigated, research remains limited in the European lowlands, particularly in central Germany. Denudation in these regions has been influenced by past periglacial processes and intensive human activities, including extensive farming and deforestation. Quantifying long-term denudation rates in these regions is therefore important for assessing the influence of climate and human activity on landscape evolution.

For this study, we collected quartz-rich samples for $^{10}$Be analysis from a low-relief catchment, the Roda Catchment, in central-eastern Germany. We constrained 17 catchment-wide and 5 local denudation rates based on the $^{10}$Be concentrations

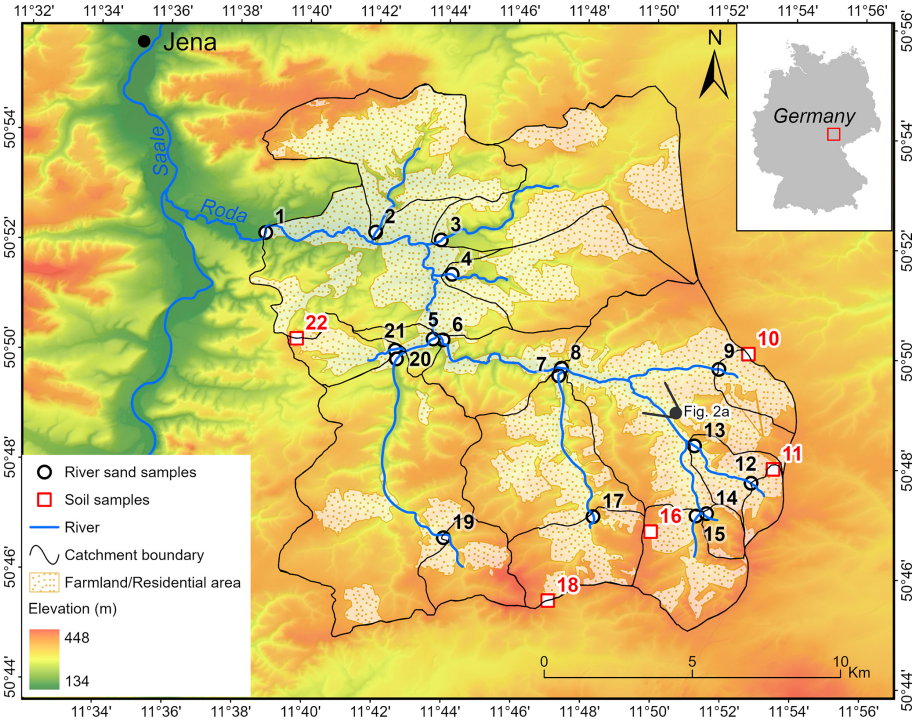


**Figure 1.** Topographic map of the Roda Catchment, showing sub-catchments, sample locations, and sample IDs next to the sample locations. Fluvial (river sand) samples are shown as black circles, and soil samples are shown as red rectangles. The black circle near sample 13 marks the viewpoint of the photo in Fig. 2a.

in river sediments and surface soils from flat catchment divides, respectively. By combining our results with global denudation records from the Octopus database (Codilean et al., 2018; Codilean et al., 2022; Codilean and Munack, 2025) and global short-term erosion rates (Chen et al., 2022), we aim to explore (1) the influence of periglacial activities on denudation by analyzing European denudation rates in the context of existing global data, (2) the impact of human activity on short- and long-term erosion rates by comparing long-term $^{10}$Be-derived denudation rates with decadal erosion rates in central Europe, and (3) long-term changes in the topographic relief of the Roda Catchment resulting from denudation.

## 2 Material and methods

### 2.1 Study area

The Roda Catchment is located a few kilometers southeast of Jena in Thuringia, Germany (Fig. 1). The Roda River is a tributary to the Saale. The bedrock within the Roda Catchment mainly consists of siliciclastic sedimentary rocks (*Buntsandstein*; Hartmann and Moosdorf, 2012). The overall relief does not exceed 260 m: the uppermost parts are mostly flat (Fig. 2d), while incision of the Roda River and its tributaries (e.g., Fig. 2e) at least partly leads to steep slopes. The climate is temperate oceanic with a mean annual temperature of ∼ 8 °C and with mean annual precipitation of ∼ 660 mm (Fick and Hijmans, 2017). The main land use types are forest and farmland (Figs. 1 and 2). KMZ files in the Supplement are provided to visualize the catchments and sampling sites in Google Earth.

### 2.2 Sampling and sample processing

A total of 22 $^{10}$Be samples were collected: 17 river sand samples and 5 soil samples (Figs. 1 and 2). River sand samples were taken from active streams. There are no extensive terraces and floodplains in the Roda Catchment, indicating low sediment storage within the catchment. Soil samples were collected from flat agricultural fields near the catchment divides. All soils are very sandy and rich in quartz.

Samples were first sieved to 250–710 µm, and quartz was enriched and purified using HCl (32 %), magnetic separation, and a mixture of 1 : 1 (by volume) of $H_2SiF_6$ (35 %) and HCl (32 %) (Brown et al., 1991; Merchel et al., 2019). We then partially dissolved the samples three times (∼ 10 % each step) using HF (48 %) to remove meteoric $^{10}$Be (Brown et al., 1991). About 0.36 mg $^{9}$Be was added to every ∼ 50 g quartz sample and processing blank. More information about our self-made $^{9}$Be carrier is provided in Appendix A. The samples were dissolved in 48 % HF at room temperature using high-density polyethylene bottles placed on a shaker table. They were then fumed three times with $HNO_3$ (> 65 %) and then three times with HCl (32 %). Thereafter, beryl-


**Figure 2.** **(a)** Photographic view of the Roda Catchment facing northwest; the viewing direction and photo location are indicated in Fig. 1. **(b)** The river from which sample 3 was collected. **(c)** Confluence of two tributaries; samples 5 and 6 were collected from the individual tributaries. **(d)** Flat catchment divide where soil sample 10 was collected. **(e)** Fluvial incision observed near sample 12. **(f)** Humanmade stone revetment upstream of sample 4.

lium was separated by anion and cation exchange chromatography and pH-selective precipitation (Merchel and Herpers, 1999), oxidized to BeO, mixed with Nb (1 : 2 by weight), and finally pressed in copper accelerator mass spectrometry (AMS) targets using Cu pins. The AMS analyses were performed at the Vienna Environmental Research Accelerator (VERA) facility with a dedicated $^{10}$Be detector described by Steier et al. (2019). The $^{10}$Be / $^{9}$Be ratios were normalized to the in-house standard SMD-Be-12 with $^{10}\mathrm{Be}/^{9}\mathrm{Be} = (1.704 \pm 0.03) \times 10^{12}$ (Akhmadaliev et al., 2013), which is traceable to the NIST 4325 standard material (Nishiizumi et al., 2007).

## 2.3 Catchment-wide denudation rate calculations

For an eroding surface, the cosmogenic nuclide concentrations in mineral grains decrease with increasing denudation rates, and for commonly used cosmogenic radioactive nuclides, $^{10}$Be and $^{26}$Al, this relationship can be described by the following equation (e.g., Lal, 1991):

$$N_i(z) = \sum_{x=\mathrm{sp,\,fm,\,sm}} \frac{P_{i,x}(0)}{\lambda_i + \frac{\varepsilon}{\Lambda_x}} \cdot e^{-\frac{z}{\Lambda_x}}, \quad (1)$$

where $N_i$ is the nuclide concentration of cosmogenic nuclide $i$ (atoms g$^{-1}$), and $z$ and $\varepsilon$ are the mass depth (g cm$^{-2}$) and

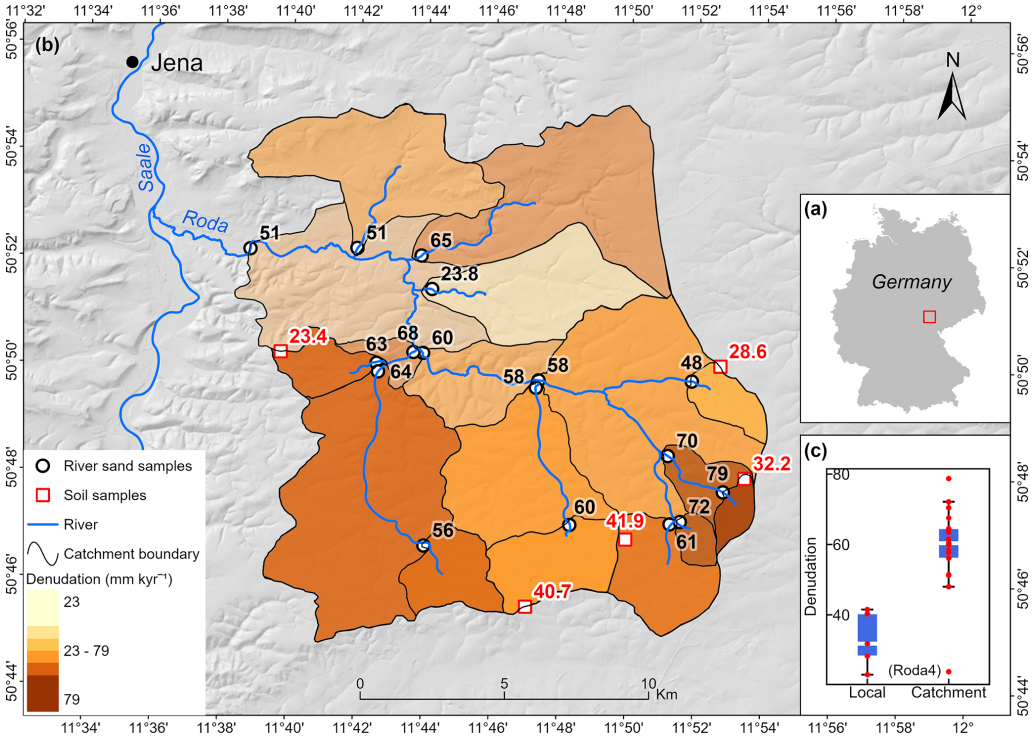


**Figure 3.** **(a)** Location of the Roda Catchment. **(b)** Calculated catchment-wide denudation rates are shown in black numbers and shaded in brown, and local denudation rates are shown in red numbers. **(c)** Boxplot for local and catchment-wide denudation rates. The white lines within the boxes indicate mean values. See Table 2 for associated uncertainties.

mass denudation rate ($\mathrm{g\,cm^{-2}\ yr^{-1}}$), respectively. $x$ stands for three nuclide production pathways: high-energy neutron spallation (sp), slow muon (sm) capture, and fast muon (fm) interactions. $P_{i,x}(0)$ is the production rate of nuclide $i$ by production pathway $x$ at the surface ($z = 0$) ($\mathrm{atoms\,g^{-1}\ yr^{-1}}$), $\lambda_i$ is the decay constant of nuclide $i$ ($\mathrm{yr^{-1}}$), and $\Lambda$ is the attenuation length of the production pathway $x$ ($\mathrm{g\,cm^{-2}}$) (Lal, 1991; Gosse and Phillips, 2001). This model assumes that (a) the production rates of cosmogenic nuclides decrease exponentially with depth in soil or rock, (b) the initial cosmogenic nuclide concentrations are negligible, (c) the denudation is in steady state, and (d) the surface has been continuously exposed to cosmic rays for a long period of time, i.e., $t \gg 1/(\lambda + \varepsilon/\Lambda)$ (e.g., Lal, 1991; Granger and Riebe, 2014; Balco, 2017; Knudsen et al., 2019).

The cosmogenic nuclide method was initially used to estimate rock surface denudation rates and soon extended to derive catchment-wide denudation rates based on the following assumptions: (a) river sediment is well mixed and representative of the entire catchment, (b) each area of the catchment contributes quartz to the river channel in proportion to its long-term denudation rate, (c) sediment storage within the catchment is negligible, (d) denudation rates are independent of sediment grain size, and (e) denudation is rapid enough that cosmogenic nuclide loss is primarily driven by denudation rather than radioactive decay (Brown et al., 1995; Bierman and Steig, 1996; Granger et al., 1996; von Blanckenburg, 2005; Granger and Riebe, 2014). Several calculators have been developed accordingly, such as CosmoCalc (Vermeesch, 2007), CRONUS-Earth (Balco et al., 2008), CAIRN (Mudd et al., 2016), BASINGA (Charreau et al., 2019), and RIVERSAND (Stübner et al., 2023).

We use the Catchment-Averaged denudatIon Rates from cosmogenic Nuclides (CAIRN), a freely available pixel-based calculator (Mudd et al., 2016), to calculate catchment-wide denudation rates. CAIRN calculates $^{10}$Be production rates for each pixel in a catchment and then uses a temporary denudation rate to obtain pixel-based $^{10}$Be concentrations and their average. CAIRN determines the catchment-wide denudation rates by adjusting this temporary denudation until the averaged $^{10}$Be concentrations match the measurements. CAIRN uses the commonly used Lal/St scaling model (Lal, 1991; Stone, 2000). The inputs to the CAIRN calculator include sample location, $^{10}$Be concentrations, and a digital elevation model (DEM) of the study area. We used a 25 m DEM for the Roda Catchment, downloaded from the geoportal Thuringia (https://geoportal.thueringen.de/gdi-th/download-offene-geodaten/download-hoehendaten, last access: 6 February 2026). The default density of $2.65\,\mathrm{g\,cm^{-3}}$ was used to allow for consistent comparison with most published denudation data. Topographic shielding corrections for catchments were automatically performed by the CAIRN

calculator. Corrections for lithology and snow shielding are not applied, as lithology (dominated by siliciclastic sedimentary rocks) and quartz content (> 50 %) are relatively homogeneous in the Roda Catchment, and snow cover is limited in both duration and thickness.

### 2.4 Local denudation rate calculations

We also use CAIRN to calculate local denudation rates for the 5 soil samples, with the same parameters to ensure consistency. In addition, due to plowing in recent decades, the top ~ 30 cm of soil is well mixed and has a density of approximately 1.3 g cm$^{-3}$. The plowing depth is equivalent to 14.7 cm of rock with a density of 2.65 g cm$^{-3}$. The sample thickness was therefore set to 14.7 cm. Topographic shielding is negligible for these high, flat sites.

### 2.5 Global datasets for comparison

To investigate denudation across different spatial and temporal scales, we combined our results with previously published short- and long-term denudation rates for comparison. The Octopus database compiles global $^{10}$Be-derived long-term denudation rates (Codilean et al., 2018, 2022; Codilean and Munack, 2025). As these rates were recalculated using CAIRN, direct comparison and integration with our data are justified. Chen et al. (2022) compiled global short-term erosion rates estimated from suspended sediment fluxes measured at gauging stations. Their Fig. 1 shows the gauging stations used worldwide. Chen et al. (2022) assumed a uniform density of 1.6 g cm$^{-3}$ to convert sediment yields to catchment-averaged erosion rates. For consistency with the $^{10}$Be-derived long-term denudation rates, we used a density of 2.65 g cm$^{-3}$ instead. In addition, as Chen et al. (2022) did not provide catchment polygons, we assigned catchment polygons from the HydroBASINS database (https://www.hydrosheds.org, last access: 6 February 2026) to each gauging station based on station locations and catchment area records in the dataset, using visual inspection in ArcGIS Pro® with satellite imagery as a basemap. Automated catchment delineation tools in ArcGIS Pro® were tested but yielded implausible catchment extents for some gauging stations; therefore, a visual assignment approach was adopted. The assigned catchments in Europe are shown in Fig. 5.

## 3 Results

AMS measurements show that the $^{10}$Be / $^{9}$Be ratios for all samples range from 120.2 to 359 × 10$^{-15}$ (Table 1). The $^{10}$Be / $^{9}$Be ratios of the three processing blanks are 4.3, 7.3, and 7.7 × 10$^{-15}$, representing < 6 % of the sample ratios. The blank-corrected $^{10}$Be concentrations range from 54.6 × 10$^{3}$ to 166.5 × 10$^{3}$ atoms g$^{-1}$ (Table 2). The derived catchment-wide denudation rates range from 23.8 ± 5.4 to 79 ± 18 mm kyr$^{-1}$ (Fig. 3 and Table 2) with an uncertainty-weighted mean denudation rate of 59.3 ± 2.8 mm kyr$^{-1}$. Sample Roda4 (23.8 ± 5.4 mm kyr$^{-1}$) indicates a much lower denudation rate than others (Fig. 3c). If this sample is omitted, the weighted mean denudation rate is 61.6 ± 2.0 mm kyr$^{-1}$. Local denudation rates are generally lower, ranging from 23.4 ± 5.6 to 41.9 ± 9.8 mm kyr$^{-1}$ with a weighted mean value of 33.5 ± 3.2 mm kyr$^{-1}$ (Fig. 3c).

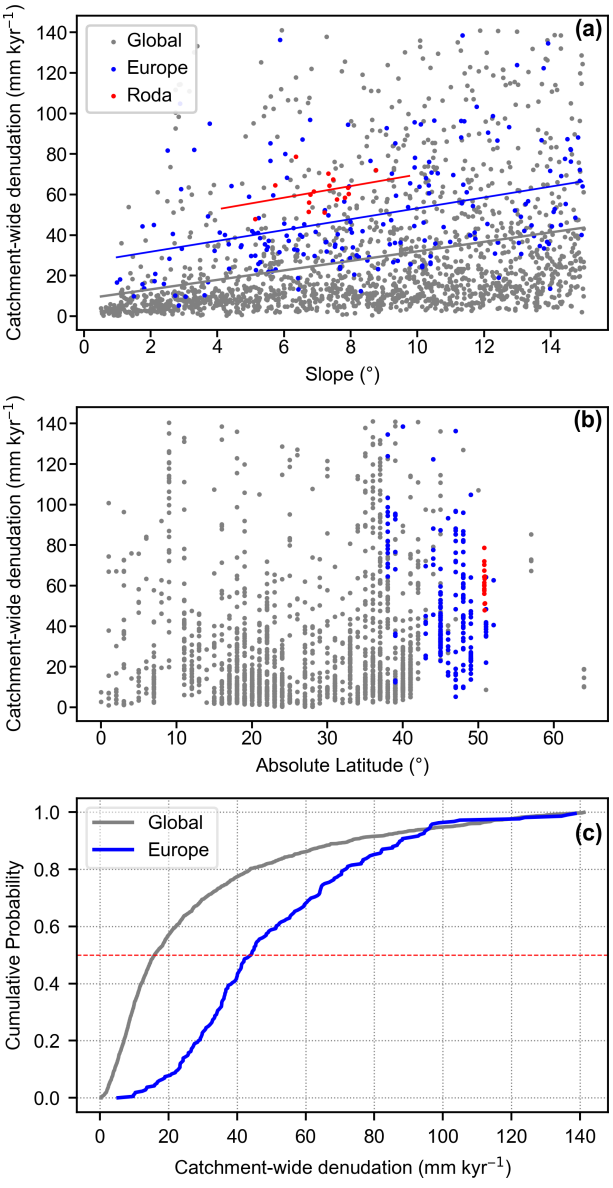


**Figure 4.** **(a)** Correlation between slope and catchment-wide denudation rates. **(b)** Correlation between latitude and denudation rates. **(c)** Cumulative distribution function (CDF) curves showing denudation rates in Europe and worldwide. Sample Roda4 is excluded from these plots because of its anomalously low denudation rate (see Fig. 3c). All subplots are based on the same dataset taken from the Octopus database (Codilean et al., 2018, 2022; Codilean and Munack, 2025).

**Table 1.** Sample coordinates and weights, $^{9}$Be weights, and measured AMS data for $^{10}$Be concentration calculations.

| Sample name | Latitude (° N) | Longitude (° E) | Quartz weight (g) | $^{9}$Be (mg) | $^{10}$Be / $^{9}$Be ratio ($\times 10^{-15}$) | $^{10}$Be / $^{9}$Be ratio of chemistry blanks ($\times 10^{-15}$) |
|---|---|---|---|---|---|---|
| River sand samples | | | | | | |
| Roda1 | 50.8695 | 11.6464 | 49.932 | 0.3549 | $174 \pm 11$ | $7.3 \pm 2.3$ |
| Roda2 | 50.8760 | 11.7044 | 49.678 | 0.3514 | $168.0 \pm 6.5$ | $4.3 \pm 1.4$ |
| Roda3 | 50.8706 | 11.7374 | 49.552 | 0.3487 | $139.0 \pm 6.1$ | $4.3 \pm 1.4$ |
| Roda4 | 50.8570 | 11.7442 | 49.843 | 0.3535 | $359 \pm 11$ | $7.3 \pm 2.3$ |
| Roda5 | 50.8363 | 11.7210 | 50.802 | 0.3501 | $137.1 \pm 7.0$ | $4.3 \pm 1.4$ |
| Roda6 | 50.8377 | 11.7322 | 39.231 | 0.3569 | $120.2 \pm 5.1$ | $7.3 \pm 2.3$ |
| Roda7 | 50.8255 | 11.7887 | 50.405 | 0.3521 | $156.7 \pm 7.5$ | $4.3 \pm 1.4$ |
| Roda8 | 50.8297 | 11.7891 | 49.193 | 0.3538 | $157.4 \pm 7.3$ | $7.3 \pm 2.3$ |
| Roda9 | 50.8300 | 11.8645 | 49.791 | 0.3508 | $189.2 \pm 8.0$ | $4.3 \pm 1.4$ |
| Roda12 | 50.7956 | 11.8807 | 50.475 | 0.3477 | $122.9 \pm 5.6$ | $4.3 \pm 1.4$ |
| Roda13 | 50.8067 | 11.8533 | 49.071 | 0.3521 | $133.1 \pm 5.7$ | $7.7 \pm 1.4$ |
| Roda14 | 50.7862 | 11.8596 | 46.560 | 0.3559 | $123.4 \pm 8.1$ | $7.3 \pm 2.3$ |
| Roda15 | 50.7854 | 11.8545 | 48.961 | 0.3521 | $152 \pm 10$ | $7.7 \pm 1.4$ |
| Roda17 | 50.7848 | 11.8053 | 51.124 | 0.3497 | $162.8 \pm 7.6$ | $7.7 \pm 1.4$ |
| Roda19 | 50.7777 | 11.7338 | 49.537 | 0.3532 | $166.3 \pm 6.2$ | $7.7 \pm 1.4$ |
| Roda20 | 50.8318 | 11.7101 | 49.865 | 0.3573 | $141.7 \pm 6.2$ | $7.3 \pm 2.3$ |
| Roda21 | 50.8344 | 11.7093 | 50.177 | 0.3549 | $139.7 \pm 5.9$ | $7.7 \pm 1.4$ |
| Soil samples | | | | | | |
| Roda10soil | 50.8347 | 11.8786 | 51.547 | 0.3504 | $292 \pm 21$ | $4.3 \pm 1.4$ |
| Roda11soil | 50.7999 | 11.8911 | 44.401 | 0.3535 | $230.0 \pm 9.1$ | $7.3 \pm 2.3$ |
| Roda16soil | 50.7805 | 11.8329 | 50.276 | 0.3532 | $205.3 \pm 9.1$ | $7.7 \pm 1.4$ |
| Roda18soil | 50.7591 | 11.7842 | 44.067 | 0.3562 | $182.4 \pm 6.6$ | $7.3 \pm 2.3$ |
| Roda22soil | 50.8375 | 11.6621 | 50.276 | 0.3532 | $337 \pm 18$ | $7.7 \pm 1.4$ |

## 4 Discussion

### 4.1 Uncertainty analysis

Before comparing our results with published denudation rates, we briefly discuss several potentially confounding factors.

First, chemical weathering occurs throughout soil, regolith, and bedrock and contributes to denudation rates. However, $^{10}$Be concentrations are mainly sensitive to near-surface mass removal (Dixon et al., 2009; Ott et al., 2022). This leads to a systematic underestimation of denudation rates. The Roda Catchment is dominated by weathering-resistant siliciclastic sedimentary rocks. Therefore, the chemical weathering effect is likely limited.

Second, catchment-wide denudation rates can be biased by sediment storage and remobilization. Ideally, river sediments at catchment outlets originate from the entire catchment, and the required time for sediment transportation is negligible compared to the time for denudation on hillslopes (e.g., von Blanckenburg, 2005; Granger and Riebe, 2014; Dosseto and Schaller, 2016). In the Roda Catchment, no vast terraces or floodplains exist. The catchment is small, and sediment transport distance is short (Fig. 1). Therefore, sediment storage and remobilization are minimal.

Third, farming may locally elevate denudation rates above long-term averages and bias catchment-wide denudation rates toward human-influenced subareas (Granger et al., 1996). This effect is likely small in the Roda Catchment because slope, the primary control on erosion, is similar between farmland (6°) and non-farmland areas (8°), and other factors, such as lithology, precipitation, and vegetation cover, are consistent across the catchment.

Fourth, other human activities, such as construction work, can disturb $^{10}$Be signals. The anomalously low denudation rate derived from sample Roda4 (Fig. 3c) may be related to extensive urban development along the upstream river reach. As illustrated in Fig. 2f, the river channel is largely modified by humanmade stone revetment constructed from abundant allochthonous lithic materials. KMZ files in the Supplement allow further inspection of anthropogenic disturbances within this catchment using Google Earth.

**Table 2.** Sample name and associated catchment characteristics (mean altitude, area, and mean slope), measured $^{10}$Be concentrations (blank-corrected), and derived denudation rates.

| Sample name | $^{10}$Be concentration ($\times 10^3$ atoms g$^{-1}$) | Mean altitude (m) | Area (km$^2$) | Mean slope (°) | Denudation (mm kyr$^{-1}$) |
|---|---|---|---|---|---|
| River sand samples | | | | | |
| Roda1 | $79.2 \pm 6.5$ | 313 | 247.1 | 7.2 | $51 \pm 12$ |
| Roda2 | $77.4 \pm 3.7$ | 286 | 22.5 | 6.7 | $51 \pm 12$ |
| Roda3 | $63.3 \pm 3.5$ | 314 | 29.4 | 5.7 | $65 \pm 15$ |
| Roda4 | $166.5 \pm 6.2$ | 312 | 17.5 | 5.2 | $23.8 \pm 5.4$ |
| Roda5 | $61.1 \pm 3.9$ | 325 | 53.7 | 7.5 | $68 \pm 16$ |
| Roda6 | $68.7 \pm 4.5$ | 334 | 96.8 | 7.9 | $60 \pm 14$ |
| Roda7 | $71.1 \pm 4.2$ | 337 | 29.9 | 7.8 | $58 \pm 13$ |
| Roda8 | $72.1 \pm 4.6$ | 340 | 86.3 | 7.6 | $58 \pm 13$ |
| Roda9 | $87 \pm 4.4$ | 348 | 4.2 | 5.1 | $48 \pm 11$ |
| Roda12 | $54.6 \pm 3.2$ | 371 | 2.4 | 6.4 | $79 \pm 18$ |
| Roda13 | $60.1 \pm 3.4$ | 356 | 6.7 | 7.3 | $70 \pm 16$ |
| Roda14 | $59.3 \pm 5.3$ | 368 | 2.1 | 8.8 | $72 \pm 17$ |
| Roda15 | $69.3 \pm 5.7$ | 369 | 10.3 | 6.9 | $61 \pm 15$ |
| Roda17 | $70.9 \pm 4.1$ | 364 | 10.3 | 6.8 | $60 \pm 14$ |
| Roda19 | $75.6 \pm 3.6$ | 365 | 7.2 | 6.7 | $56 \pm 13$ |
| Roda20 | $64.4 \pm 4.1$ | 333 | 46.6 | 7.4 | $64 \pm 15$ |
| Roda21 | $62.4 \pm 3.5$ | 279 | 4.8 | 7.9 | $63 \pm 15$ |
| Soil samples | | | | | |
| Roda10soil | $130.7 \pm 10$ | 360 | – | 0 | $28.6 \pm 6.9$ |
| Roda11soil | $118.5 \pm 6.1$ | 378 | – | 0 | $31.2 \pm 7.5$ |
| Roda16soil | $92.7 \pm 5.0$ | 391 | – | 0 | $41.9 \pm 9.8$ |
| Roda18soil | $94.6 \pm 4.8$ | 382 | – | 0 | $40.7 \pm 9.5$ |
| Roda22soil | $154.6 \pm 9.1$ | 330 | – | 0 | $23.4 \pm 5.6$ |

### 4.2 Comparison of denudation rates in Europe and globally

The catchment-wide denudation rates in the Roda Catchment fall within the range of existing European data (Fig. 4a). Denudation rates from the Roda Catchment, Europe, and around the globe show similar slope dependence (Fig. 4a). Global data, including European records, are sourced from the Octopus database. European data represent denudation rates in relatively high latitude (Fig. 4b). The cumulative distribution function (CDF) plot indicates that denudation rates in Europe are much higher than global rates, with a CDF 0.5 value $> 40$ mm kyr$^{-1}$ and thus more than twice the global value (Fig. 4c).

The European data range from 30 to 65 mm kyr$^{-1}$, representing the 25th and 75th percentiles, respectively. These rates integrate averaging timescales of approximately 9 to 20 ka (von Blanckenburg, 2005), extending back into the last glacial period. During this time period, Europe experienced widespread glaciation and extensive periglacial processes, including cryoturbation and solifluction (Isarin and Renssen, 1999; Eissmann, 2002). Syntheses of European periglacial geomorphology indicate that frost-related processes extended far beyond glacier margins, affecting large ice-free lowland areas of northern and central Europe (e.g., Oliva et al., 2022). Palaeopermafrost reconstructions further demonstrate that periglacial conditions were widespread across large parts of western and central Europe during the Last Glacial Maximum (e.g., Vandenberghe and Pissart, 1993). Consistent with geomorphological and palaeopermafrost evidence, the widespread cover-bed sequences on slopes between 37 and 56° N indicate that periglacial processes once affected large parts of the European continent during the Quaternary (Kleber, 1997). The periglacial processes may have altered landscape erodibility and potentially increased denudation rates across Europe (Schaller et al., 2001; Delunel et al., 2010; Roda-Boluda et al., 2023). Therefore, the generally higher denudation rates from Europe are probably due to past glacial and periglacial dynamics.

### 4.3 Comparison of long-term denudation and short-term erosion rates in Europe

We compare $^{10}$Be-derived long-term denudation rates with gauged short-term erosion rates in Europe (Fig. 5) to investigate denudation on different timescales. Results show that long-term denudation rates are positively correlated with slope (Fig. 6a). The short-term erosion rates display greater

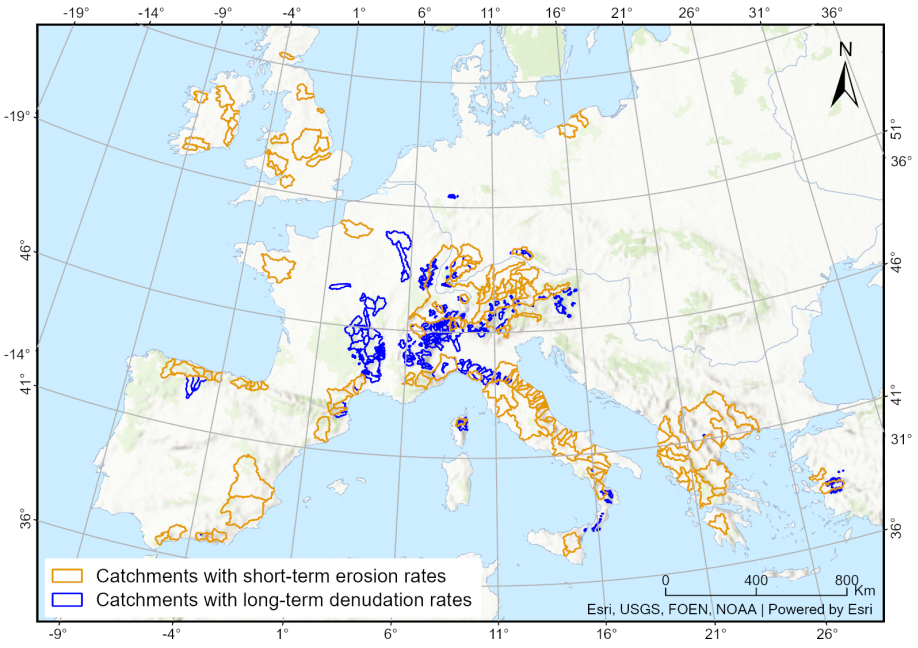


**Figure 5.** Catchments with long-term denudation (Octopus data, Codilean et al., 2018) or short-term erosion rates (Chen et al., 2022) in central Europe.

variability than the long-term denudation rates (Fig. 6a). This likely documents human activities, such as deforestation, farming, mining, and quarrying (Ferrier et al., 2005). Those activities are more stochastic compared to natural denudation drivers, such as topographic gradient and precipitation. As a result, human activity may lead to great variability in short-term erosion rates and a weaker correlation between slope and erosion rates (Fig. 6a). The variability decreases for slopes $> 20°$, probably because human activities are relatively weak in steep regions.

The CDF plot indicates that $^{10}$Be-derived long-term denudation rates are generally higher than the short-term erosion rates in Europe (Fig. 6b). This observation is consistent with Chen et al. (2022). Many factors can lead to this pattern. The first reason is the difference between gauged erosion rates and $^{10}$Be-derived denudation rates. Denudation rates derived from cosmogenic nuclides represent the total mass loss by physical removal of particles and chemical removal of solutes (von Blanckenburg, 2005; Granger and Riebe, 2014). The gauged measurements used account for only suspended sediment flux and miss the dissolved mass loss. Studies have shown that chemical weathering can even dominate denudation rates in limestone or carbonate settings (e.g., Ott et al., 2023; Schaller et al., 2025).

However, chemical weathering may not be the only or main reason for this pattern (Fig. 6b). $^{10}$Be-derived long-term denudation rates average over timescales of thousands of years, while gauged measurements cover only decades and usually cannot capture rare extreme heavy floods (Kirchner et al., 2001; Schaller et al., 2001; Meyer et al., 2010a; Granger and Riebe, 2014).

Moreover, land-cover changes in Europe over the last several thousand years need to be considered. Reconstructions of land-cover change show that Europe experienced extensive forest clearance during the Roman and Medieval periods, reflecting agricultural expansion and the exploitation of forests for fuel wood and construction materials (Kaplan et al., 2009). This deforestation has been widely linked to enhanced hillslope erosion and increased sediment fluxes recorded in fluvial and lacustrine archives across Europe (Dotterweich, 2008, 2012). A synthesis of global erosion-rate data further indicates that human activities can accelerate natural erosion rates by a factor of $\sim$ 2–3 under moderate land use and by up to an order of magnitude under intensive land use (Saunders and Young, 1983). Together with the geomorphic legacy of periglacial processes during the last glacial period, widespread anthropogenic disturbances may have also contributed to long-term denudation rates exceeding short-term erosion rates (Fig. 6b).

### 4.4 Topographic relief changes in the Roda Catchment

In the Roda Catchment, we constrained both catchment-wide and local denudation rates on catchment divides. The mean catchment-wide denudation rate is $\sim 62\,\mathrm{mm\,kyr^{-1}}$ (if we treat sample Roda4 as an outlier), which is much higher than the mean local denudation rate of $\sim 34\,\mathrm{mm\,kyr^{-1}}$. The averaging timescales are about 10 and 18 kyr, respectively, so we can assess changes in topographic relief since then. At face

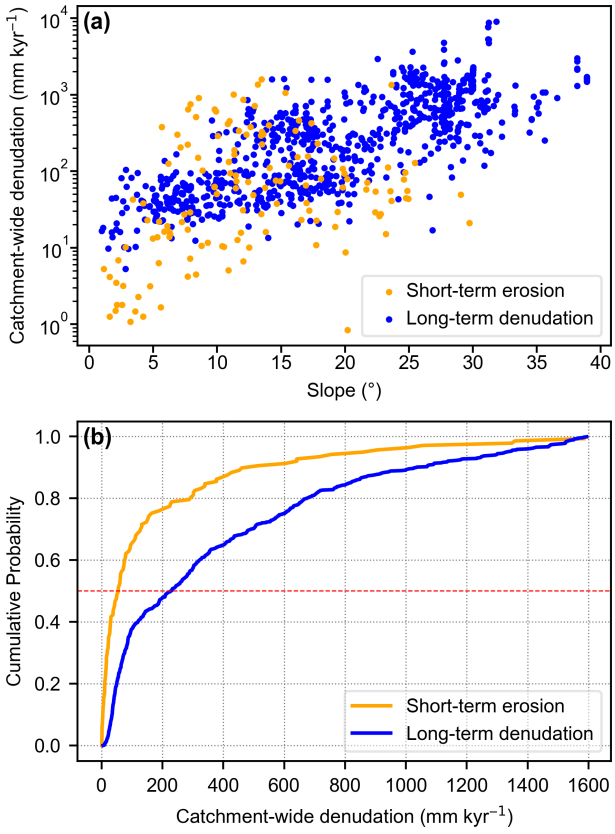


**Figure 6.** **(a)** Correlation between slope and long-term denudation rates (blue) and short-term erosion rates (orange) in Europe. **(b)** CDF curves for both long-term denudation rates and short-term erosion rates. The red dashed horizontal line indicates that the CDF 0.5 value increases significantly from ∼ 50 to > 200 mm kyr$^{-1}$. The data correspond to the catchments shown in Fig. 5.

value, the average surface lowering rate in the catchment area exceeds that at the catchment divides by 28 mm kyr$^{-1}$.

However, a relatively thick soil layer has been observed at the catchment divides. Assuming that all eroded material was soil with a density of 1.3 g cm$^{-3}$, this would result in a mean denudation rate of 69 mm kyr$^{-1}$, rather than 34 mm kyr$^{-1}$. Consequently, the results indicate that denudation may have contributed to relief changes in the Roda Catchment, ranging from ∼ 0 to 28 mm kyr$^{-1}$. This relief change is broadly consistent with the observations in the Harz Mountain (5–10 mm kyr$^{-1}$) (Hetzel et al., 2024) and the Black Forest (24 mm kyr$^{-1}$) in Germany (Meyer et al., 2010b).

## 5 Conclusions

This paper presents $^{10}$Be-derived catchment-wide and local denudation rates for the Roda Catchment in central Germany. The derived denudation rates indicate that the Roda Catchment erodes at a mean rate of ∼ 62 mm kyr$^{-1}$, which is much higher than the mean denudation rate of 34 mm kyr$^{-1}$ observed at the catchment divides. In combination with published long-term denudation rates and short-term erosion rates, we explored the roles of periglacial conditions and anthropogenic disturbance in driving denudation and landscape evolution. We argue that the generally high long-term denudation rates in Europe are likely due to periglacial processes during the last glacial period and the massive forest clearance during Roman and Medieval times. These factors can also help explain why long-term denudation rates exceed short-term erosion rates observed in Europe. Moreover, rare but extreme events are likely important for long-term denudation. Denudation has resulted in an average topographic relief change of 0 to 28 mm kyr$^{-1}$ in the Roda Catchment over the past 10 ka.

## Appendix A: Preparation of our $^{9}$Be carrier solution from a phenakite crystal

We prepared our Be carrier from a phenakite crystal from Kragerö, Norway, which was kindly provided by the Geosciences Collections, TU Bergakademie Freiberg. The procedure follows that of Merchel et al. (2013):

1. *Grinding, dissolution, and dryness*. We ground the phenakite crystal and then treated the phenakite powder with HF (48 %) and a small amount of $HNO_3$ (70 %) in a high-density polyethylene bottle. The bottle was placed at room temperature in an ultrasonic bath during the day and on a shaker table at night. A few days later, over 80 % of the material was dissolved, and the decanted solution was evaporated to dryness.

2. *Be purification by fuming*. We treated the evaporated solution remains with warm water for several hours (Stone, 1998) and centrifuged the solution to remove insoluble compounds. The solution was then evaporated to dryness and treated with HF (48 %) three times to fume off boron trifluoride ($BF_3$), which was followed by addition and evaporation of $HClO_4$ (70 %) to destroy all remaining fluorides. The residue was then dissolved in HCl (7.1 mol L$^{-1}$).

3. *Be purification by precipitation*. We gradually added $NH_3$aq (32 %) to the HCl solution until pH 4 was reached, and the generated hydroxides (e.g., $Ti(OH)_2$, $Fe(OH)_3$) were separated from the solution by centrifugation. Further addition of $NH_3$aq (32 %) precipitated beryllium hydroxide, which was washed three times with dilute $NH_3$aq (pH 8–9) and then redissolved in HCl (18 %), obtaining the Be carrier solution.

4. *Concentration measurements*. We measured the concentration of the Be carrier in three laboratories using either inductively coupled plasma optical emission spectrometry (ICP-OES) or inductively coupled plasma mass spectrometry (ICP-MS). Calibration was done against

various dilutions of a commercial Be standard (LGC Standards). Table A1 presents all measurement results. The density ($1.0259 \pm 0.0017\,g\,mL^{-1}$) was determined by comparing measured $^{9}Be$ carrier mass to that of a deionized water sample (assumed to be $1.0\,g\,mL^{-1}$), using equal volumes for both across five replicates. This allows the calculation of the $^{9}Be$ concentration from $3511 \pm 52\,mg\,L^{-1}$ (Table A1) to $3422 \pm 51\,mg\,kg^{-1}$. The uncertainty is derived from the standard error of the mean of both water and the $^{9}Be$ carrier, and it is small (1 order of magnitude lower than the one from the ICP) compared to the overall uncertainty.

**Table A1.** Concentration of Be carrier measured in different laboratories.

| Laboratories | Concentration ($mg\,L^{-1}$) |
|---|---|
| Institute of Geography, Friedrich Schiller University Jena (ICP-OES) | $3485 \pm 67$ |
| Institute of Geoscience, Friedrich Schiller University Jena (ICP-MS) | $3620 \pm 155$ |
| Monuments Preservation and Archaeology, Thuringian State Office, Germany (ICP-MS) | $3525 \pm 100$ |
| Weighted mean | $3511 \pm 52$ |

**Data availability.** All data are available in the paper.

**Supplement.** The supplement related to this article is available online at https://doi.org/10.5194/egqsj-75-19-2026-supplement.

**Author contributions.** LZ and RZ designed the study and collected the samples. LZ processed the samples with assistance from SM. OM and AW conducted the measurements. The paper was written by LZ, RZ, and YL, with contributions from all co-authors.

**Competing interests.** The contact author has declared that none of the authors has any competing interests.

**Disclaimer.** Publisher's note: Copernicus Publications remains neutral with regard to jurisdictional claims made in the text, published maps, institutional affiliations, or any other geographical representation in this paper. The authors bear the ultimate responsibility for providing appropriate place names. Views expressed in the text are those of the authors and do not necessarily reflect the views of the publisher.

**Acknowledgements.** This research is a contribution to the International Research Training Group "Geo-ecosystems in transition on the Tibetan Plateau (TransTiP)", funded by the Deutsche Forschungsgemeinschaft (DFG grant 317513741/GRK 2309). AMS measurements were supported by the RADIATE project under grant agreement 824096 from the EU Research and Innovation program Horizon 2020. We thank the VERA team, especially Martin Martschini and Peter Steier, for AMS support. We are grateful to Michael Gäbelein from the Geosciences Collections, TU Bergakademie Freiberg, for providing the phenakite; Christopher Berndt and Nico Blaubach (Institute of Geography, FSU Jena) for preparing the Be carrier solution; and Dirk Merten (Institute for Geosciences, FSU Jena) and Oliver Mecking (Thüringer Landesamt für Denkmalpflege und Archäologie) for measuring the Be concentrations. We thank Alissa Flatley and the anonymous reviewer for their constructive feedback, which has improved this paper.

**Financial support.** This research has been supported by the Deutsche Forschungsgemeinschaft (grant no. 317513741/GRK 2309) and the Horizon 2020 (grant no. 824096).

**Review statement.** This paper was edited by Jan-Hendrik May and reviewed by Alissa Flatley and one anonymous referee.

## References


Akhmadaliev, S., Heller, R., Hanf, D., Rugel, G., and Merchel, S.: The new 6MV AMS-facility DREAMS at Dresden, Nucl. Instrum. Methods Phys. Res., Sect. B, 294, 5–10, https://doi.org/10.1016/j.nimb.2012.01.053, 2013.

Allen, P. A.: From landscapes into geological history, Nature, 451, 274–276, https://doi.org/10.1038/nature06586, 2008.

Balco, G.: Production rate calculations for cosmic-ray-muon-produced $^{10}$Be and $^{26}$Al benchmarked against geological calibration data, Quat. Geochronol., 39, 150–173, https://doi.org/10.1016/j.quageo.2017.02.001, 2017.

Balco, G., Stone, J. O., Lifton, N. A., and Dunai, T. J.: A complete and easily accessible means of calculating surface exposure ages or erosion rates from $^{10}$Be and $^{26}$Al measurements, Quat. Geochronol., 3, 174–195, https://doi.org/10.1016/j.quageo.2007.12.001, 2008.

Bierman, P. and Steig, E. J.: Estimating rates of denudation using cosmogenic isotope abundances in sediment, Earth Surf. Process. Landf., 21, 125–139, https://doi.org/10.1002/(SICI)1096-9837(199602)21:2<125::AID-ESP511>3.0.CO;2-8, 1996.

Bierman, P. and Turner, J.: $^{10}$Be and $^{26}$Al evidence for exceptionally low rates of Australian bedrock erosion and the likely existence of Pre-Pleistocene landscapes, Quat. Res., 44, 378–382, https://doi.org/10.1006/qres.1995.1082, 1995.

Brown, E. T., Edmond, J. M., Raisbeck, G. M., Yiou, F., Kurz, M. D., and Brook, E. J.: Examination of surface exposure ages of Antarctic moraines using in situ produced $^{10}$Be and $^{26}$Al, Geochim. Cosmochim. Acta, 55, 2269–2283, https://doi.org/10.1016/0016-7037(91)90103-C, 1991.

Brown, E. T., Stallard, R. F., Larsen, M. C., Raisbeck, G. M., and Yiou, F.: Denudation rates determined from the accumulation of in situ-produced $^{10}$Be in the luquillo experimental forest, Puerto Rico, Earth Planet. Sci. Lett., 129, 193–202, https://doi.org/10.1016/0012-821X(94)00249-X, 1995.

Carretier, S., Regard, V., Vassallo, R., Aguilar, G., Martinod, J., Riquelme, R., Pepin, E., Charrier, R., Hérail, G., Farías, M., Guyot, J.-L., Vargas, G., and Lagane, C.: Slope and climate variability control of erosion in the Andes of central Chile, Geology, 41, 195–198, https://doi.org/10.1130/G33735.1, 2013.

Charreau, J., Blard, P. H., Zumaque, J., Martin, L., Delobel, T., and Szafran, L.: BASINGA: A cell-by-cell GIS toolbox for computing BASIN averaGe scaling factors, cosmogenic production rates and denudation rAtes, Earth Surf. Process. Landf., 44, https://doi.org/10.1002/esp.4649, 2019.

Chen, S.-A., Michaelides, K., Richards, D. A., and Singer, M. B.: Exploring exogenous controls on short- versus long-term erosion rates globally, Earth Surf. Dynam., 10, 1055–1078, https://doi.org/10.5194/esurf-10-1055-2022, 2022.

Clayton, J. L. and Megahan, W. F.: Erosional and chemical denudation rates in the Southwestern Idaho batholith, Earth Surf. Process. Landf., 11, 389–400, https://doi.org/10.1002/esp.3290110405, 1986.

Codilean, A. T. and Munack, H.: Short communication: Updated CRN Denudation collections in OCTOPUS v2.3, Geochronology, 7, 113–122, https://doi.org/10.5194/gchron-7-113-2025, 2025.

Codilean, A. T., Munack, H., Cohen, T. J., Saktura, W. M., Gray, A., and Mudd, S. M.: OCTOPUS: an open cosmogenic isotope and luminescence database, Earth Syst. Sci. Data, 10, 2123–2139, https://doi.org/10.5194/essd-10-2123-2018, 2018.

Codilean, A. T., Munack, H., Saktura, W. M., Cohen, T. J., Jacobs, Z., Ulm, S., Hesse, P. P., Heyman, J., Peters, K. J., Williams, A. N., Saktura, R. B. K., Rui, X., Chishiro-Dennelly, K., and Panta, A.: OCTOPUS database (v.2), Earth Syst. Sci. Data, 14, 3695–3713, https://doi.org/10.5194/essd-14-3695-2022, 2022.

Delunel, R., van der Beek, P. A., Carcaillet, J., Bourlès, D. L., and Valla, P. G.: Frost-cracking control on catchment denudation rates: Insights from in situ produced $^{10}$Be concentrations in stream sediments (Ecrins–Pelvoux massif, French Western Alps), Earth Planet. Sci. Lett., 293, 72–83, https://doi.org/10.1016/j.epsl.2010.02.020, 2010.

Delunel, R., Schlunegger, F., Valla, P. G., Dixon, J., Glotzbach, C., Hippe, K., Kober, F., Molliex, S., Norton, K. P., Salcher, B., Wittmann, H., Akçar, N., and Christl, M.: Late-Pleistocene catchment-wide denudation patterns across the European Alps, Earth Sci. Rev., 211, 103407, https://doi.org/10.1016/j.earscirev.2020.103407, 2020.

Dixon, J. L., Heimsath, A. M., and Amundson, R.: The critical role of climate and saprolite weathering in landscape evolution, Earth Surf. Process. Landf., 34, 1507–1521, https://doi.org/10.1002/esp.1836, 2009.

Dosseto, A. and Schaller, M.: The erosion response to Quaternary climate change quantified using uranium isotopes and in situ-produced cosmogenic nuclides, Earth Sci. Rev., 155, 60–81, https://doi.org/10.1016/j.earscirev.2016.01.015, 2016.

Dotterweich, M.: The history of soil erosion and fluvial deposits in small catchments of central Europe: Deciphering the long-term interaction between humans and the environment – A review, Geomorphology, 101, 192–208, https://doi.org/10.1016/j.geomorph.2008.05.023, 2008.

Dotterweich, M.: Past soil erosion in central Europe: Human impact and long term effects, eTopoi, 3, 39–45, 2012.

Eissmann, L.: Quaternary geology of eastern Germany (Saxony, Saxon–Anhalt, South Brandenburg, Thüringia), type area of the Elsterian and Saalian Stages in Europe, Quat. Sci. Rev., 21, 1275–1346, https://doi.org/10.1016/S0277-3791(01)00075-0, 2002.

Ferrier, K. L., Kirchner, J. W., and Finkel, R. C.: Erosion rates over millennial and decadal timescales at Caspar Creek and Redwood Creek, Northern California Coast Ranges, Earth Surf. Process. Landf., 30, 1025–1038, https://doi.org/10.1002/esp.1260, 2005.

Fick, S. E. and Hijmans, R. J.: WorldClim 2: new 1-km spatial resolution climate surfaces for global land areas, Int. J. Climatol., 37, 4302–4315, https://doi.org/10.1002/joc.5086, 2017.

Gosse, J. C. and Phillips, F. M.: Terrestrial in situ cosmogenic nuclides: theory and application, Quat. Sci. Rev., 20, 1475–1560, https://doi.org/10.1016/S0277-3791(00)00171-2, 2001.

Granger, D. E. and Riebe, C. S.: 7.12 – Cosmogenic Nuclides in Weathering and Erosion, in: Treatise on Geochemistry, 2nd edn., edited by: Holland, H. D. and Turekian, K. K., Elsevier, Oxford, 401–436, https://doi.org/10.1016/B978-0-08-095975-7.00514-3, 2014.

Granger, D. E., Kirchner, J. W., and Finkel, R.: Spatially averaged long-term erosion rates measured from in situ-produced cosmogenic nuclides in alluvial sediment, The Journal of Geology, 104, 249–257, http://www.jstor.org/stable/30068190 (last access: 6 February 2026), 1996.

Hancock, G. and Kirwan, M.: Summit erosion rates deduced from $^{10}$Be: Implications for relief production in the central Appalachians, Geology, 35, 89–92, https://doi.org/10.1130/G23147A.1, 2007.

Hartmann, J. and Moosdorf, N.: The new global lithological map database GLiM: A representation of rock properties at the Earth surface, Geochem. Geophys. Geosyst., 13, https://doi.org/10.1029/2012GC004370, 2012.

Heineke, C., Hetzel, R., Nilius, N.-P., Glotzbach, C., Akal, C., Christl, M., and Hampel, A.: Spatial patterns of erosion and landscape evolution in a bivergent metamorphic core complex revealed by cosmogenic $^{10}$Be: The central Menderes Massif (western Turkey), Geosphere, 15, 1846–1868, https://doi.org/10.1130/GES02013.1, 2019.

Hetzel, R., Rother, H., Wolff, R., and Hölzer, K.: Millennial-scale erosion rates in the Harz Mountains (Germany) from cosmogenic $^{10}$Be: implications for landscape evolution of basement highs in Central Europe, E&G Quaternary Sci. J., 73, 161–178, https://doi.org/10.5194/egqsj-73-161-2024, 2024.

Isarin, R. F. B. and Renssen, H.: Reconstructing and modelling Late Weichselian climates: the Younger Dryas in Europe as a case study, Earth Sci. Rev., 48, 1–38, https://doi.org/10.1016/S0012-8252(99)00047-1, 1999.

Kaplan, J. O., Krumhardt, K. M., and Zimmermann, N.: The prehistoric and preindustrial deforestation of Europe, Quat. Sci. Rev., 28, 3016–3034, https://doi.org/10.1016/j.quascirev.2009.09.028, 2009.

Kirchner, J. W., Finkel, R. C., Riebe, C. S., Granger, D. E., Clayton, J. L., King, J. G., and Megahan, W. F.: Mountain erosion over 10 yr, 10 k.y., and 10 m.y. time scales, Geology, 29, 591–594, https://doi.org/10.1130/0091-7613(2001)029<0591:MEOYKY>2.0.CO;2, 2001.

Kleber, A.: Cover-beds as soil parent materials in midlatitude regions, CATENA, 30, 197–213, https://doi.org/10.1016/S0341-8162(97)00018-0, 1997.

Knudsen, M. F., Egholm, D. L., and Jansen, J. D.: Time-integrating cosmogenic nuclide inventories under the influence of variable erosion, exposure, and sediment mixing, Quat. Geochronol., 51, 110–119, https://doi.org/10.1016/j.quageo.2019.02.005, 2019.

Lal, D.: Cosmic ray labeling of erosion surfaces: in situ nuclide production rates and erosion models, Earth Planet. Sci. Lett., 104, 424–439, https://doi.org/10.1016/0012-821X(91)90220-C, 1991.

Lenzi, M. A. and Marchi, L.: Suspended sediment load during floods in a small stream of the Dolomites (northeastern Italy), CATENA, 39, 267–282, https://doi.org/10.1016/S0341-8162(00)00079-5, 2000.

Li, Y., Li, D., Liu, G., Harbor, J., Caffee, M., and Stroeven, A. P.: Patterns of landscape evolution on the central and northern Tibetan Plateau investigated using in-situ produced $^{10}$Be concentrations from river sediments, Earth Planet. Sci. Lett., 398, 77–89, https://doi.org/10.1016/j.epsl.2014.04.045, 2014.

Merchel, S. and Herpers, U.: An Update on Radiochemical Separation Techniques for the Determination of Long-Lived Radionuclides via Accelerator Mass Spectrometry, Radiochim. Acta, 84, 215–220, https://doi.org/10.1524/ract.1999.84.4.215, 1999.

Merchel, S., Bremser, W., Bourlès, D. L., Czeslik, U., Erzinger, J., Kummer, N. A., Leanni, L., Merkel, B., Recknagel, S., and Schaefer, U.: Accuracy of $^{9}$Be-data and its influence on $^{10}$Be cosmogenic nuclide data, Radioanal. Nucl. Chem., 298, 1871–1878, https://doi.org/10.1007/s10967-013-2746-x, 2013.

Merchel, S., Gärtner, A., Beutner, S., Bookhagen, B., and Chabilan, A.: Attempts to understand potential deficiencies in chemical procedures for AMS: Cleaning and dissolving quartz for $^{10}$Be and $^{26}$Al analysis, Nucl. Instrum. Methods Phys. Res., Sect. B, 455, 293–299, https://doi.org/10.1016/j.nimb.2019.02.007, 2019.

Meyer, H., Hetzel, R., and Strauss, H.: Erosion rates on different timescales derived from cosmogenic $^{10}$Be and river loads: implications for landscape evolution in the Rhenish Massif, Germany, Int. J. Earth Sci., 99, 395–412, https://doi.org/10.1007/s00531-008-0388-y, 2010a.

Meyer, H., Hetzel, R., Fügenschuh, B., and Strauss, H.: Determining the growth rate of topographic relief using in situ-produced $^{10}$Be: A case study in the Black Forest, Germany, Earth Planet. Sci. Lett., 290, 391–402, https://doi.org/10.1016/j.epsl.2009.12.034, 2010b.

Milliman, J. D. and Meade, R. H.: World-wide delivery of river sediment to the oceans, The Journal of Geology, 91, 1–21, https://doi.org/10.1086/628741, 1983.

Mishra, A. K., Placzek, C., and Jones, R.: Coupled influence of precipitation and vegetation on millennial-scale erosion rates derived from $^{10}$Be, PLOS ONE, 14, e0211325, https://doi.org/10.1371/journal.pone.0211325, 2019.

Mudd, S. M., Harel, M.-A., Hurst, M. D., Grieve, S. W. D., and Marrero, S. M.: The CAIRN method: automated, reproducible calculation of catchment-averaged denudation rates from cosmogenic nuclide concentrations, Earth Surf. Dynam., 4, 655–674, https://doi.org/10.5194/esurf-4-655-2016, 2016.

Nishiizumi, K., Lal, D., Klein, J., Middleton, R., and Arnold, J. R.: Production of $^{10}$Be and $^{26}$Al by cosmic rays in terrestrial quartz in situ and implications for erosion rates, Nature, 319, 134–136, https://doi.org/10.1038/319134a0, 1986.

Nishiizumi, K., Imamura, M., Caffee, M. W., Southon, J. R., Finkel, R. C., and McAninch, J.: Absolute calibration of $^{10}$Be AMS standards, Nucl. Instrum. Methods Phys. Res., Sect. B, 258, 403–413, https://doi.org/10.1016/j.nimb.2007.01.297, 2007.

Oliva, M., Nývlt, D., and Fernández-Fernández, J. M. (Eds.): Periglacial landscapes of Europe, Springer Cham, XII, 523 pp., https://doi.org/10.1007/978-3-031-14895-8, 2022.

Ott, R., Gallen, S. F., and Helman, D.: Erosion and weathering in carbonate regions reveal climatic and tectonic drivers of carbonate landscape evolution, Earth Surf. Dynam., 11, 247–257, https://doi.org/10.5194/esurf-11-247-2023, 2023.

Ott, R. F.: How Lithology Impacts Global Topography, Vegetation, and Animal Biodiversity: A Global-Scale Analysis of Mountainous Regions, Geophys. Res. Lett., 47, e2020GL088649, https://doi.org/10.1029/2020GL088649, 2020.

Ott, R. F., Gallen, S. F., and Granger, D. E.: Cosmogenic nuclide weathering biases: corrections and potential for denudation and weathering rate measurements, Geochronology, 4, 455–470, https://doi.org/10.5194/gchron-4-455-2022, 2022.

Palumbo, L., Hetzel, R., Tao, M., and Li, X.: Topographic and lithologic control on catchment-wide denudation rates derived from cosmogenic $^{10}$Be in two mountain ranges at the margin of NE Tibet, Geomorphology, 117, 130–142, https://doi.org/10.1016/j.geomorph.2009.11.019, 2010.

Portenga, E. W. and Bierman, P. R.: Understanding Earth's eroding surface with $^{10}$Be, GSA Today, 21, 4–10, https://doi.org/10.1130/G111A.1, 2011.

Riebe, C. S., Kirchner, J. W., Granger, D. E., and Finkel, R. C.: Strong tectonic and weak climatic control of long-term chemical weathering rates, Geology, 29, 511–514, https://doi.org/10.1130/0091-7613(2001)029<0511:STAWCC>2.0.CO;2, 2001.

Roda-Boluda, D. C., Schildgen, T. F., Wittmann, H., Tofelde, S., Bufe, A., Prancevic, J., and Hovius, N.: Elevation-dependent periglacial and paraglacial processes modulate tectonically-controlled erosion of the western southern Alps, New Zealand, J. Geophys. Res.-Earth Surf., 128, e2023JF007271, https://doi.org/10.1029/2023JF007271, 2023.

Saunders, I. and Young, A.: Rates of surface processes on slopes, slope retreat and denudation, Earth Surf. Process. Landf., 8, 473–501, https://doi.org/10.1002/esp.3290080508, 1983.

Schaller, M., von Blanckenburg, F., Hovius, N., and Kubik, P. W.: Large-scale erosion rates from in situ-produced cosmogenic nuclides in European river sediments, Earth Planet. Sci. Lett., 188, 441–458, https://doi.org/10.1016/S0012-821X(01)00320-X, 2001.

Schaller, M., Peifer, D., Neely, A. B., Bernard, T., Glotzbach, C., Beer, A. R., and Ehlers, T. A.: Spatiotemporal denudation rates of the Swabian Alb escarpment (southwestern Germany) dominated by anthropogenic impact, lithology, and base-level lowering, Earth Surf. Dynam., 13, 571–591, https://doi.org/10.5194/esurf-13-571-2025, 2025.

Scharf, T. E., Codilean, A. T., de Wit, M., Jansen, J. D., and Kubik, P. W.: Strong rocks sustain ancient postorogenic topography in southern Africa, Geology, 41, 331–334, https://doi.org/10.1130/G33806.1, 2013.

Starke, J., Ehlers, T. A., and Schaller, M.: Latitudinal effect of vegetation on erosion rates identified along western South America, Science, 367, 1358–1361, https://doi.org/10.1126/science.aaz0840, 2020.

Steier, P., Martschini, M., Buchriegler, J., Feige, J., Lachner, J., Merchel, S., Michlmayr, L., Priller, A., Rugel, G., Schmidt, E., Wallner, A., Wild, E. M., and Golser, R.: Comparison of methods for the detection of $^{10}$Be with AMS and a new approach based on a silicon nitride foil stack, Int. J. Mass Spectrom., 444, 116175, https://doi.org/10.1016/j.ijms.2019.116175, 2019.

Stone, J.: A Rapid Fusion Method for Separation of Beryllium-10 From Soils and Silicates, Geochim. Cosmochim. Acta, 62, 555–561, https://doi.org/10.1016/S0016-7037(97)00340-2, 1998.

Stone, J. O.: Air pressure and cosmogenic isotope production, J. Geophys. Res.: Solid Earth, 105, 23753–23759, https://doi.org/10.1029/2000JB900181, 2000.

Stübner, K., Balco, G., and Schmeisser, N.: RIVERSAND: A new tool for efficient computation of catchmentwide erosion rates, Radiocarbon, 1–14, https://doi.org/10.1017/RDC.2023.74, 2023.

Vandenberghe, J. and Pissart, A.: Permafrost changes in Europe during the last glacial, Permafrost Periglac. Process., 4, 121–135, https://doi.org/10.1002/ppp.3430040205, 1993.

Vermeesch, P.: CosmoCalc: An Excel add-in for cosmogenic nuclide calculations, Geochem. Geophys. Geosyst., 8, https://doi.org/10.1029/2006GC001530, 2007.

von Blanckenburg, F.: The control mechanisms of erosion and weathering at basin scale from cosmogenic nuclides in river sediment, Earth Planet. Sci. Lett., 237, 462–479, https://doi.org/10.1016/j.epsl.2005.06.030, 2005.

Wolff, R., Hetzel, R., and Strobl, M.: Quantifying river incision into low-relief surfaces using local and catchment-wide $^{10}$Be denudation rates, Earth Surf. Process. Landf., 43, 2327–2341, https://doi.org/10.1002/esp.4394, 2018.